
Radial Structure of Shell Modulations Near Peak Compression of Spherical Implosions

Introduction

In inertial confinement fusion (ICF), a spherical target is imploded by either direct illumination of laser beams (direct drive)¹ or x rays produced in a high-Z enclosure (hohlraum).² The growth of shell perturbations is the greatest factor limiting target performance in these implosions. Initial nonuniformities in the shell include target imperfections and modulations from laser nonuniformities in the case of direct-drive ICF.^{3–8} These modulations initially grow at the shell's outer surface during the laser-driven part of implosions due to the acceleration-phase Rayleigh–Taylor (RT) instability^{9–12} and convergent Bell–Plesset (BP) effects.¹³ These outer-surface perturbations feed through the shell during their acceleration-phase growth, seeding the deceleration-phase RT instability^{14–18} on the inner surface. As the shell starts to decelerate, the outer-shell modulations become stable. The inner surface of the shell, however, is subject to the RT instability during the deceleration phase since the higher-density shell is slowed down by the lower-density gas of the target core.^{14–18} As a result, the shell modulations penetrate deep into the gas fuel region causing shell–fuel mixing.^{19–21} This mixing inhibits the achievement of high compression and reduces the fuel temperature that is necessary to sustain efficient fuel burn.

The first measurements^{18,22} of shell modulations around peak compression were based on differential imaging²² of core emission with shells having diagnostic titanium-doped layers. At peak compression, when the maximum density and temperature occur, the hot, compressed core and inner surface of the shell produce strong x-ray emission. This emission is used as a backlighter to probe the outer, colder shell.²² To measure shell integrity, both time-integrated²² and time-resolved¹⁸ measurements used imaging at photon energies above and below the titanium *K* edge. Core images at photon energies below the *K* edge (not absorbed by the shell) provide the spatial shape of the backlighter, while core images at photon energies above the *K* edge (highly absorbed by the shell's titanium) contain information about the structure of shell-area-density modulations in the titanium-doped layer.

Earlier experiments^{18,22} were limited to measurements of perturbations at the shell's inner surface, where modulations and compression were expected to be the highest. Measurements with titanium-doped layers placed in the central and outer parts of the shell were not sensitive enough to detect perturbations. Differential imaging in the current experiments is extended to the much more sensitive absorption in the titanium *1s–2p* spectral region instead of the absorption above the *K* edge. Near peak compression, the shell is heated by energy transported from the hot core through thermal conduction and radiation. At temperatures around 0.1 to 1 keV, the shell titanium is partially ionized and is able to absorb core radiation not only at photon energies above the *K* edge (≥ 4.966 keV) but also in the *1s–2p* absorption line region at photon energies around 4.5 to 4.75 keV. The mass absorption rate of any absorption line from the titanium *1s–2p* spectral region is about one order of magnitude higher than at photon energies above the *K* edge. As a result, differential imaging can be extended to the central and outer parts of the shell, where the compression and modulations are smaller. In this article the first measurements of the compressed-shell modulation structure away from the inner surface are presented. A similar technique has also been employed for modulation measurements in indirectly driven implosions.²³

Experimental Conditions

Figure 92.1 shows a schematic of spherical targets and the positions of the titanium-doped layers in the shell used in these experiments and their predicted location at peak compression. Targets with $\sim 450\text{-}\mu\text{m}$ initial radii and $20\text{-}\mu\text{m}$ -thick shells, filled with 18 atm of D^3He gas, were imploded by 351-nm laser light using the 60-beam OMEGA laser system²⁴ with a 1-ns square pulse and a total energy of ~ 23 kJ. All shots were taken with laser beams smoothed by distributed phase plates (DPP's),²⁵ 1-THz, two-dimensional smoothing by spectral dispersion (2-D SSD),²⁶ and polarization smoothing (PS)²⁷ using birefringent wedges. The average beam-to-beam energy imbalance was $\sim 3\%$ in all implosions. The diagnostic, $1\text{-}\mu\text{m}$ -thick, titanium-doped ($\sim 2\%$ by atom) CH layers were offset

from the inner surface by $\sim 1, 5, 7,$ and $9 \mu\text{m}$ of pure CH. These layers were expected to determine shell-areal-density modulations at the inner, central, and outer parts of the shell at peak compression. Figure 92.1(b) shows the temperature and density profiles at peak compression of one of the targets calculated by the 1-D code *LILAC*.²⁸ At peak compression, the diagnostic titanium layer offset by $1 \mu\text{m}$ is located on the slope of the density profile at the inner shell, where the unstable surface is located. Titanium layers offset by $5 \mu\text{m}$ and $7 \mu\text{m}$ are in the central part of the shell, and the layer offset by $9 \mu\text{m}$ lies in the outer part of the shell at peak compression [see Fig. 92.1(b)].

Core images were measured with a gated monochromatic x-ray imager (GMXI),²⁹ which was set up for time-integrated (~ 200 -ps) measurements during these experiments. One channel of the GMXI recorded monochromatic (with FWHM of ~ 30 eV) images at ~ 4.60 keV in the spectral region of titanium $1s-2p$ absorption, while the other channel was set up at ~ 4.87 keV outside titanium absorption regions or emission lines. Figure 92.2 shows Wiener-filtered images³⁰ for shots with titanium layers offset by $1, 5, 7,$ and $9 \mu\text{m}$ and for one shot without titanium, which was used to estimate the noise level. The Wiener filter used a noise level constructed from the difference of two images $I_{1s-2p}(\mathbf{r})$ and $I_{<K}(\mathbf{r})$ in shot

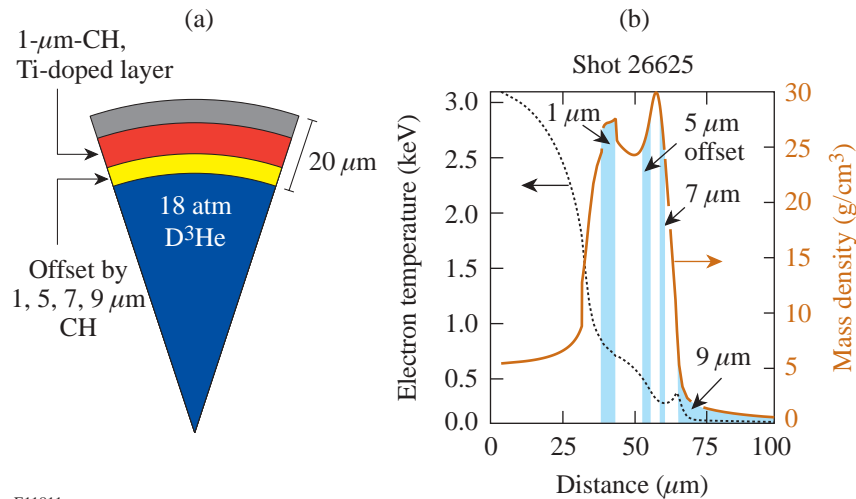
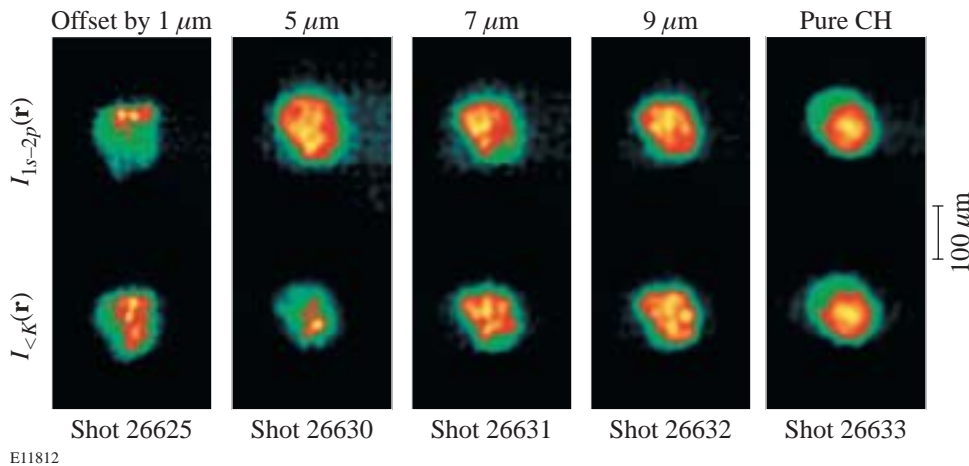


Figure 92.1

(a) Schematic of spherical targets with diagnostic titanium-doped (2% by atom) layers offset by $1, 5, 7,$ and $9 \mu\text{m}$ of pure CH from the inner surface. (b) *LILAC*-simulated profiles of target density and temperature at peak compression of the implosion. The locations of titanium-doped layers are shown by the light blue areas.

E11811



E11812

Figure 92.2

Wiener-filtered core images around peak compression at energies inside (~ 4.60 keV, upper row of images) and outside (~ 4.87 keV, lower row of images) the titanium $1s-2p$ absorption spectral region for shots with $1\text{-}\mu\text{m}$ - (shot 26625), $5\text{-}\mu\text{m}$ - (shot 26630), $7\text{-}\mu\text{m}$ - (shot 26631), and $9\text{-}\mu\text{m}$ -offset (shot 26632) titanium-doped layers, and for the shot without titanium (26633).

26633 without titanium and the measured GMXI modulation transfer function (MTF).³¹ All the details of the image processing are described in Refs. 18, 22, and 30. The shell optical-depth (OD) modulations were calculated using the natural logarithm of the ratio of intensities of the two images at photon energies in the $1s-2p$ spectral region (highly absorbed by the shell), $I_{1s-2p}(\mathbf{r})$, and outside the $1s-2p$ region, below the K edge (weakly absorbed by the shell), $I_{<K}(\mathbf{r})$:

$$\delta[\text{OD}(\mathbf{r})] = \delta\left\{\ln\left[I_{1s-2p}(\mathbf{r})/I_{<K}(\mathbf{r})\right]\right\}.$$

The spectra of the core emissions were captured on an x-ray streak camera.³² They were subsequently time integrated and used to infer a spatial average of the OD of the titanium layer in the $1s-2p$ spectral region. The red line (shot 26625) in Fig. 92.3(a) shows an example of a measured time-integrated spectrum $S_{\text{meas}}(E)$ as a function of photon energy E . The spectral responses of the GMXI at two channels in $[R_{1s-2p}(E)]$ and out $[R_{<K}(E)]$ of the $1s-2p$ absorption spectral region are represented by the dashed and dotted lines, respectively. The thick green line represents the estimated continuum level $S_{\text{con}}(E)$ of core x rays, used to calculate average titanium optical depth $\text{OD} = \ln[S_{\text{con}}(E)/S_{\text{meas}}(E)]$ at a photon energy of $E = 4.6$ keV. The average titanium OD is used to determine the relative OD modulations (which are equal to the relative areal-density modulations), $\delta[\text{OD}(\mathbf{r})]/\text{OD} = \delta[\rho R(\mathbf{r})]/\rho R$, to compare levels of modulations in the different parts of the shell.

In addition, the measured spectra are used to calculate the spatial variations in images due to small variations in the spectral response across the vertical axis of the images. For example, the central part of the image $I_{1s-2p}(\mathbf{r})$ is set up for measurements at a photon energy of $E = 4.60$ keV. The x rays originating at this point of the image are reflected at an angle

of $5.88 \pm 0.01^\circ$ from the GMXI multilayer mirror. The x rays originating from the horizontal line at $100 \mu\text{m}$ off the image center are reflected from the mirror at a slightly different angle of $5.91 \pm 0.01^\circ$, corresponding to a photon energy of 4.58 keV. Similarly, the x rays originating at the horizontal line at $-100 \mu\text{m}$ off the center line in the image plane are reflected from the mirror at an angle of $5.85 \pm 0.01^\circ$, corresponding to a photon energy of 4.63 keV. The resulting image correction functions were calculated for each shot using corresponding spectra. For example, for the images at the $1s-2p$ absorption channel, the resulting correction function is proportional to the convolution of the measured spectrum $S_{\text{meas}}(E)$ with the spectral response function $R_{1s-2p}(E)$. Figure 92.3(b) shows correction functions for shot 26625 inside (dashed line) and outside (dotted line) the $1s-2p$ absorption channel. For each Wiener-filtered image, the x-ray intensity at the vertical axis was divided by the corresponding correction function to compensate for these spatial variations.

Experimental Results

Figure 92.4 presents the images of optical-depth modulations in the titanium-doped layers offset by 1, 5, 7, and $9 \mu\text{m}$ from the shell's inner surface. As shown in Fig. 92.1(b), these layers represent different parts of the shell ranging from the inner to the outer surfaces at peak compression. Power-per-mode spectra of these modulations as functions of spatial frequency are presented in Fig. 92.5(a). The amplitudes of modulations are highest at a spatial frequency of $\sim 20 \text{ mm}^{-1}$ corresponding to a wavelength of $\sim 50 \mu\text{m}$ (with a mode number of $\ell \sim 6$). This result is in agreement with previous inner-surface measurements using K -edge imaging. The absolute values of optical-depth modulation σ_{rms} decreased monotonically from 0.30 ± 06 at the inner surface to 0.13 ± 06 at the outer surface as shown by the solid line in Fig. 92.5(b). The relative areal-

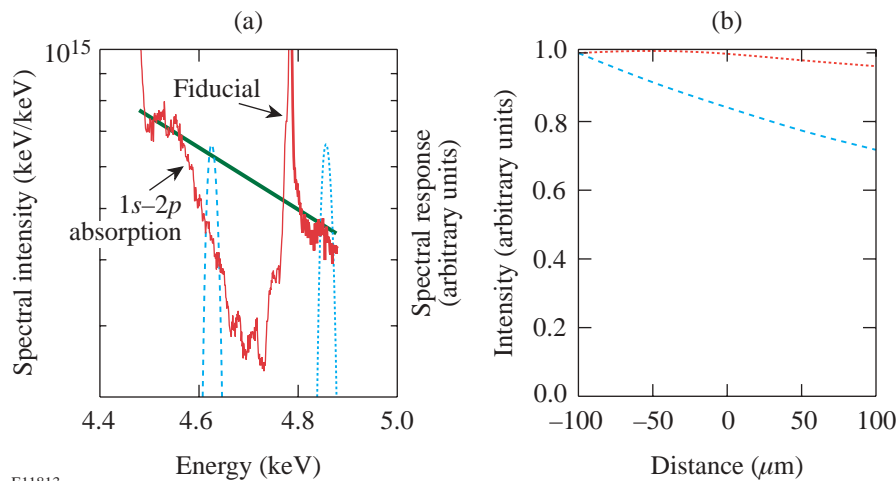


Figure 92.3

(a) Measured time-integrated spectrum $S_{\text{meas}}(E)$ as a function of photon energy for shot 26625 (red line). Estimated continuum level $S_{\text{con}}(E)$ as a function of photon energy (thick green line). The instrumental spectral responses as functions of photon energy of GMXI channels inside $[R_{1s-2p}(E)$, dashed line] and outside $[R_{<K}(E)$, dotted line] the titanium $1s-2p$ absorption region. (b) The spatial correction functions as a function of distance in the vertical axis for images inside (dashed line) and outside (dotted line) the titanium $1s-2p$ absorption region.

E11813

density modulation σ_{rms} is $59 \pm 14\%$, $18 \pm 5\%$, $26 \pm 10\%$, and $52 \pm 20\%$ in the layers offset by 1, 5, 7, and 9 μm , respectively, as shown by the dashed line in Fig. 92.5(b). The modulations are highest at the inner surface (in the 1- μm -offset layer), which is unstable during the deceleration phase of implosion near peak compression. As expected, the modulations decrease in the bulk of the shell (in the 5- and 7- μm -offset layers) but then increase at the outer surface (in the 9- μm -offset layer), which was unstable during the acceleration, laser-driven phase of the implosion. The areal-density modulations in the whole shell are dominated by nonuniformities in the inner and central parts of the shell. The contribution of outer shell modulations is small because of the small compression at the outer surface. As shown in Fig. 92.1(b), the 9- μm -offset layer is expected to be outside the compressed shell, and therefore its high modulation level is not very important to the integrity of the whole shell. The measured level of modulation at the inner surface, $59 \pm 14\%$, is in agreement with previous results²² measured at

peak compression. For comparison, at peak neutron production, ~ 100 ps earlier than the peak compression, previous time-resolved measurements have shown lower modulation levels, about 20% at the inner surface.¹⁸ In the future, experiments will extend the time-integrated measurements of modulations in the central and outer parts of the shell to time-resolved measurements using the same titanium $1s-2p$ absorption technique.

Conclusions

This article has presented the first time-integrated measurements of the compressed-shell modulation structure away from the inner surface. The differential imaging technique has replaced previous titanium K -edge imaging with much more sensitive imaging using the titanium $1s-2p$ absorption spectral region. As a result, measurements of modulations at central and outer parts of the shell have become accessible. In implosions with the 20- μm -thick shells, the relative areal-density modulation σ_{rms} is $59 \pm 14\%$, $18 \pm 5\%$, $26 \pm 10\%$, and $52 \pm 20\%$, in layers offset by 1, 5, 7, and 9 μm , respectively. The spatial spectra of modulations peaked at a spatial frequency of $\sim 20 \text{ mm}^{-1}$ corresponding to a wavelength of $\sim 50 \mu\text{m}$ (with a mode number of $\ell \sim 6$). The areal-density modulations in the whole shell are dominated by modulations in the inner and central parts of the shell, while the contribution of outer shell modulations is small because of the smaller compression at the outer surface.

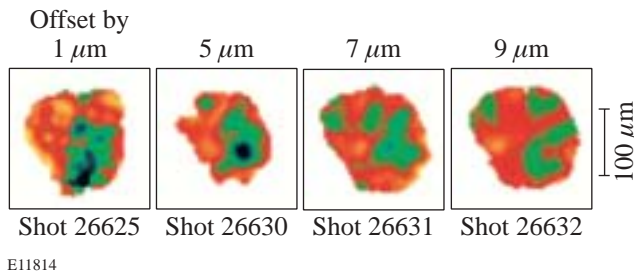


Figure 92.4
Optical-depth-modulation images at peak compression for shots with 1- μm - (shot 26625), 5- μm - (shot 26630), 7- μm - (shot 26631), and 9- μm -offset (shot 26632) titanium-doped layers integrated over ~ 200 ps of x-ray emission.

ACKNOWLEDGMENT

This work was supported by the U.S. Department of Energy Office of Inertial Confinement Fusion under Cooperative Agreement No. DE-FC03-92SF19460, the University of Rochester, and the New York State Energy Research and Development Authority. The support of DOE does not constitute an endorsement by DOE of the views expressed in this article.

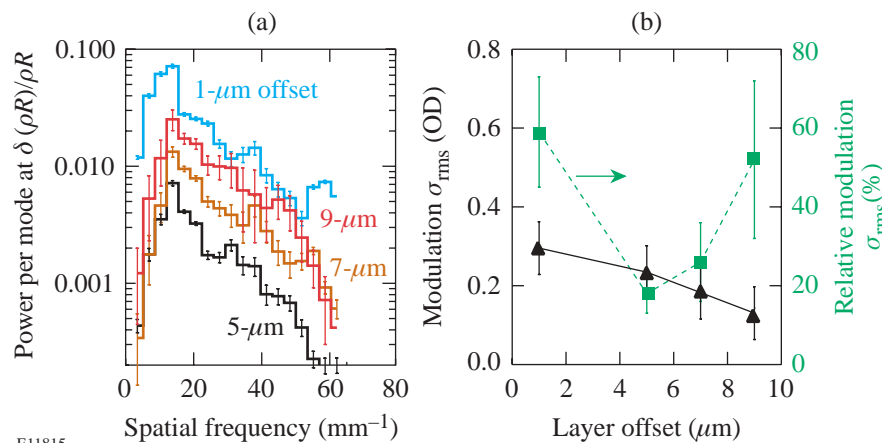


Figure 92.5
(a) Power per mode as a function of spatial frequency of relative areal-density modulations at peak compression for shots with 1-, 5-, 7-, and 9- μm -offset titanium-doped layers. (b) Peak compression optical-depth modulation σ_{rms} (solid line) and relative areal-density modulation σ_{rms} (dashed line) as functions of the layer offset.

E11815

REFERENCES

1. J. Nuckolls *et al.*, *Nature* **239**, 139 (1972).
2. J. D. Lindl, *Inertial Confinement Fusion: The Quest for Ignition and Energy Gain Using Indirect Drive* (Springer-Verlag, New York, 1998), Chap. 6, pp. 61–82.
3. C. J. Pawley *et al.*, *Phys. Plasmas* **6**, 565 (1999).
4. H. Azechi *et al.*, *Phys. Plasmas* **4**, 4079 (1997).
5. R. J. Taylor *et al.*, *Phys. Rev. Lett.* **76**, 1643 (1996).
6. D. H. Kalantar, M. H. Key, L. B. Da Silva, S. G. Glendinning, B. A. Remington, J. E. Rothenberg, F. Weber, S. V. Weber, E. Wolftrum, N. S. Kim, D. Neely, J. Zhang, J. S. Wark, A. Demir, J. Lin, R. Smith, G. J. Tallents, C. L. S. Lewis, A. MacPhee, J. Warwick, and J. P. Knauer, *Phys. Plasmas* **4**, 1985 (1997).
7. V. A. Smalyuk, T. R. Boehly, D. K. Bradley, V. N. Goncharov, J. A. Delettrez, J. P. Knauer, D. D. Meyerhofer, D. Oron, and D. Shvarts, *Phys. Rev. Lett.* **81**, 5342 (1998).
8. T. R. Boehly, V. N. Goncharov, O. Gotchev, J. P. Knauer, D. D. Meyerhofer, D. Oron, S. P. Regan, Y. Srebro, W. Seka, D. Shvarts, S. Skupsky, and V. A. Smalyuk, *Phys. Plasmas* **8**, 2331 (2001).
9. S. G. Glendinning, S. N. Dixit, B. A. Hammel, D. H. Kalantar, M. H. Key, J. D. Kilkenny, J. P. Knauer, D. M. Pennington, B. A. Remington, R. J. Wallace, and S. V. Weber, *Phys. Rev. Lett.* **78**, 3318 (1997).
10. K. S. Budil *et al.*, *Phys. Rev. Lett.* **76**, 4536 (1996).
11. K. S. Budil *et al.*, *Phys. Plasmas* **8**, 2344 (2001).
12. J. P. Knauer, R. Betti, D. K. Bradley, T. R. Boehly, T. J. B. Collins, V. N. Goncharov, P. W. McKenty, D. D. Meyerhofer, V. A. Smalyuk, C. P. Verdon, S. G. Glendinning, D. H. Kalantar, and R. G. Watt, *Phys. Plasmas* **7**, 338 (2000).
13. M. S. Plesset and T. P. Mitchell, *Q. Appl. Math.* **13**, 41 (1956).
14. H. Sakagami and K. Nishihara, *Phys. Rev. Lett.* **65**, 432 (1990).
15. R. P. J. Town and A. R. Bell, *Phys. Rev. Lett.* **67**, 1863 (1991).
16. M. C. Herrmann, M. Tabak, and J. D. Lindl, *Phys. Plasmas* **8**, 2296 (2001).
17. R. Betti, K. Anderson, V. N. Goncharov, R. L. McCrory, D. D. Meyerhofer, S. Skupsky, and R. P. J. Town, *Phys. Plasmas* **9**, 2277 (2002).
18. V. A. Smalyuk, J. A. Delettrez, V. N. Goncharov, F. J. Marshall, D. D. Meyerhofer, S. P. Regan, T. C. Sangster, R. P. J. Town, and B. Yaakobi, *Phys. Plasmas* **9**, 2738 (2002).
19. S. P. Regan, J. A. Delettrez, F. J. Marshall, J. M. Soures, V. A. Smalyuk, B. Yaakobi, V. Yu. Glebov, P. A. Jaanimagi, D. D. Meyerhofer, P. B. Radha, W. Seka, S. Skupsky, C. Stoeckl, R. P. J. Town, D. A. Haynes, Jr., I. E. Golovkin, C. F. Hooper, Jr., J. A. Frenje, C. K. Li, R. D. Petrasso, and F. H. Séguin, *Phys. Rev. Lett.* **89**, 085003 (2002).
20. D. D. Meyerhofer, J. A. Delettrez, R. Epstein, V. Yu. Glebov, V. N. Goncharov, R. L. Keck, R. L. McCrory, P. W. McKenty, F. J. Marshall, P. B. Radha, S. P. Regan, S. Roberts, W. Seka, S. Skupsky, V. A. Smalyuk, C. Sorce, C. Stoeckl, J. M. Soures, R. P. J. Town, B. Yaakobi, J. D. Zuegel, J. Frenje, C. K. Li, R. D. Petrasso, D. G. Hicks, F. H. Séguin, K. Fletcher, S. Padalino, M. R. Freeman, N. Izumi, R. Lerche, T. W. Phillips, and T. C. Sangster, *Phys. Plasmas* **8**, 2251 (2001).
21. P. B. Radha, J. Delettrez, R. Epstein, V. Yu. Glebov, R. Keck, R. L. McCrory, P. McKenty, D. D. Meyerhofer, F. Marshall, S. P. Regan, S. Roberts, T. C. Sangster, W. Seka, S. Skupsky, V. Smalyuk, C. Sorce, C. Stoeckl, J. Soures, R. P. J. Town, B. Yaakobi, J. Frenje, C. K. Li, R. Petrasso, F. Séguin, K. Fletcher, S. Padalino, C. Freeman, N. Izumi, R. Lerche, and T. W. Phillips, *Phys. Plasmas* **9**, 2208 (2002).
22. B. Yaakobi, V. A. Smalyuk, J. A. Delettrez, F. J. Marshall, D. D. Meyerhofer, and W. Seka, *Phys. Plasmas* **7**, 3727 (2000).
23. J. Koch, Lawrence Livermore National Laboratory, private communication (2002).
24. T. R. Boehly, D. L. Brown, R. S. Craxton, R. L. Keck, J. P. Knauer, J. H. Kelly, T. J. Kessler, S. A. Kumpan, S. J. Loucks, S. A. Letzring, F. J. Marshall, R. L. McCrory, S. F. B. Morse, W. Seka, J. M. Soures, and C. P. Verdon, *Opt. Commun.* **133**, 495 (1997).
25. Y. Lin, T. J. Kessler, and G. N. Lawrence, *Opt. Lett.* **20**, 764 (1995).
26. S. P. Regan, J. A. Marozas, J. H. Kelly, T. R. Boehly, W. R. Donaldson, P. A. Jaanimagi, R. L. Keck, T. J. Kessler, D. D. Meyerhofer, W. Seka, S. Skupsky, and V. A. Smalyuk, *J. Opt. Soc. Am. B* **17**, 1483 (2000).
27. T. R. Boehly, V. A. Smalyuk, D. D. Meyerhofer, J. P. Knauer, D. K. Bradley, R. S. Craxton, M. J. Guardalben, S. Skupsky, and T. J. Kessler, *J. Appl. Phys.* **85**, 3444 (1999).
28. J. Delettrez, R. Epstein, M. C. Richardson, P. A. Jaanimagi, and B. L. Henke, *Phys. Rev. A* **36**, 3926 (1987).
29. F. J. Marshall and J. A. Oertel, *Rev. Sci. Instrum.* **6**, 735 (1997).
30. V. A. Smalyuk, T. R. Boehly, L. S. Iwan, T. J. Kessler, J. P. Knauer, F. J. Marshall, D. D. Meyerhofer, C. Stoeckl, B. Yaakobi, and D. K. Bradley, *Rev. Sci. Instrum.* **72**, 635 (2001).
31. F. J. Marshall, M. M. Allen, J. P. Knauer, J. A. Oertel, and T. Archuleta, *Phys. Plasmas* **5**, 1118 (1998).
32. D. H. Kalantar *et al.*, *Rev. Sci. Instrum.* **72**, 751 (2001).